Geometric Approach to Segmentation and Protein Localization in Cell Culture Assays

S. Raman, C.A. Maxwell, M.H. Barcellos-Hoff, and B. Parvin

sraman@lbl.gov parvin@media.lbl.gov *

August 1, 2006

Abstract

Cell-based fluorescence imaging assays are heterogeneous and require the collection of a large number of images for detailed quantitative analysis. Complexities arise as a result of variation in spatial nonuniformity, shape, overlapping compartments, and scale (size). A new technique and methodology has been developed and tested for delineating subcellular morphology and partitioning overlapping compartments at multiple scales. This system is packaged as an integrated software platform for quantifying images that are obtained through fluorescence microscopy. Proposed methods are model-based, leveraging geometric shape properties of subcellular compartments and corresponding protein localization. From the morphological perspective, convexity constraint is imposed to delineate and partition nuclear compartments. From the protein localization perspective, radial symmetry is imposed to localize punctate protein events at sub-micron resolution. Convexity constraint is imposed against boundary information, which are extracted through a combination of zero-crossing and gradient operator. If the convexity constraint fails for the boundary then positive curvature maxima are

*The Research was supported by National Aeronautics and Space Administration Grant no. T6275W, NASA Specialized Center for Research in Radiation Health Effects, and the low dose radiation research program at the Office of Biological Effects Research, U.S. Department of Energy, Grant No. DE-FG03-01ER63240. C.A. Maxwell was supported by a post-doctoral multidisciplinary award (BC050612) from the Department of Defense Breast Cancer Research Program (BCRP).

localized along the contour and the entire blob is partitioned into disjointed convex objects representing individual nuclear compartment, by enforcing geometric constraints. Nuclear compartments provide the context for protein localization, which may be diffuse or punctate. Punctate signal are localized through iterative voting and radial symmetries for improved reliability and robustness. The technique has been tested against 196 images that were generated to study centrosome abnormalities. Corresponding computed representations are compared against manual counts for validation.

1 Introduction

The response of tissues and biological material in general to exogenous stimuli is often heterogeneous and requires a large set of samples for each experimental variable, e.g., tissue type, type of stimuli, dosage, and concentration. These responses are often multidimensional and multispectral and can be imaged using different types of microscopy. Quantitative analysis of these responses is a necessary step toward visualization of large scale co-localization studies and construction of predictive models. Research in this area has spanned from learning techniques using texture-based features for characterizing patterns of protein expression (Murphy, 2004) to geometric techniques using nonlinear diffusion (Malladi & Sethian, 1996; Yang & Parvin, 2003), curve evolution, and shape regularization for segmentation of subcellular compartments (Solorzano et al., 2001, Yang & Parvin, 2003; Parvin et al., 2003), and often segmentation provides context for quantifying protein expression. However, when protein expression is not diffused within a compartment, additional processing is needed within the specific context. This paper outlines a complete methodology and its evaluation for quantitative assessment of co-localization studies in cell culture assays. Although the technique has been tested against studying centrosomal abnormalities (CA), it is extensible to other phenotypic studies. As CA occur in less than 2% of normal tissue and in about 80% of breast cancers (Salisbury et al., 2004). CA may serve as valuable prognostic and therapeutic targets. Various cellular stresses, such as viral infection, exposure to ionizing radiation and altered

microenvironmental stimuli, can augment the frequency and type of CA (Salisbury, 2001). Within resting animal cells, the centrosome represents a major microtubule organizing center and is composed of a pair of centrosomes and pericentriolar material. Prior to division, the centrosome will replicate during the DNA synthesis phase of the cell cycle. During mitosis, replicated centrosomes will separate and nucleate a bipolar spindle that equally contacts and segregates the replicated genetic information into two daughter cells. One facet of CA refers to additional centrosomes (more than two), which leads to abnormal cell division. As CA are rare events in cell culture assays, large numbers of samples within and between treatment groups must be analyzed for objective results. Complexities arise as a result of nonuniform staining, overlapping nuclei, touching centrioles, and scales (size) of these subcellular compartments. In the proposed system, these complexities are addressed through model-based techniques that are driven by the inherent geometries. These geometric constraints take advantage of the convexity features of the nuclear compartment and the radial symmetry of the centrosome. Nuclear extraction is initiated from differential spatial operators as opposed to intensity thresholding, which is a common practice in most ad-hoc solutions. These differential operators lead to edge fragments that are linked for high-level geometric analysis, partitioning, and grouping. Nuclear regions provide context for quantitative protein localization. When localization is not diffused, additional analysis is required to characterize punctate signals. These punctate signals may vary in shape, scale, and intensity. Furthermore, they often overlap and create additional complexity. These complexities are addressed through iterative spatial voting, which is kernel-based, and its topography favors radial symmetries. It is robust with respect to variation in size and intensity, and delineates overlapped compartments.

Organization of this paper is as follows. Section 2 outlines material and methods. Section 3 reviews previous research. Section 4 summarizes geometric segmentation of the nuclear regions which provide the context for protein localization. Section 5 outlines the spatial voting technique for protein localization. Section 6 provides (1)the experimental results for 196 images, and (2) the comparison of the system

performance against manual analysis.

2 Material and method

The model system for the cell culture is MCF-10A (ATCC, Manassas, VA) human mammary epithelial cells (HMEC), which were grown in serum-free media as recommended by ATCC. Cells were irradiated with 100cGy within 6 hours of seeding by using 320 KvP X-ray; control plates were processed identically to irradiated plates. Media were supplemented with exogenous TGF-β(0.5 ng-per-ml) at plating and centrosomal amplification was measured 22 hours post irradiation. Cells were methanol-fixed, blocked with 0.5% casein and PBS, and centrosomes were detected with a mouse monoclonal antibody recognizing γ-tubulin (Sigma, St. Louis, MO). Co-staining with a rabbit polyclonal recognizing CENP-F, kindly provided by G. Chan, University of Alberta, Canada, and previously characterized (Chani et al., 1999), was used to determine cell cycle stage as indicated. Secondary antibodies (Molecular Probes, Carlsbad, CA) were incubated sequentially for 1 h at RT, washed, and counterstained with DAPI before mounting with Vectashield mounting medium (Vector Labs, Burlingame, CA). Image acquisition and processing immunofluorescence images for in vitro analyses were obtained using a 40X objective with 1.3 numerical aperture Zeiss Neofluar objective on a Zeiss Axiovert equipped with epifluorescence. Images were acquired by locating nuclei using the DAPI image without reference to the fluorochrome-labeled γ-tubulin. Centrosome number and structure were manually monitored as previously described (Pihan et al., 1998). Cellular treatments were blind coded in order to avoid experimental bias.

3 Previous work

The difficulties in localization of subcellular compartments are often due to variations in scale, noise, and topology. Other complexities originate from missing data and perceptual boundaries that lead to

diffusion and dispersion of the spatial grouping in the object space. Techniques for extraction of nuclear compartments are either through global thresholding or adaptive (localized) thresholding followed by the watershed (Vincent & Soille, 1991) method for separating adjacent regions. Techniques in radial symmetries, as evidenced by centrosome configuration, can be classified into three different categories: (1) point operations leading to dense output, (2) clustering based on parameterized shape models or voting schemes, and (3) iterative techniques. Point operations are usually a series of cascade filters that are tuned for radial symmetries. These techniques use image gradient magnitudes and orientations to infer the center of mass for regions of interest (Reisfeld et al., 1995; Reisfeld & Yeshurun, 1998; Sela & Levine, 1997). Recent efforts have focused on speed and reliability (Loy & Zelinsky, 2003). Parametric clustering techniques are often based on a variant of the Hough transform, *e.g.,* circle or ellipse finders. These techniques produce loci of points corresponding to the parametric models of well-known geometries. These point distributions are then merged, and model parameters are refined (Duda & Hart, 1972). Non-parametric clustering techniques operate along the gradient direction to search for radial symmetry, using either line- or area-based search. Line-based search (Minor & Sklansky, 1981) is also known as the spoke filter, where the frequency of occurrence of points normal to the edge direction is aggregated. In contrast, area-based voting accumulates votes in a small neighborhood along the gradient direction. An example of iterative method is the regularized centroid transform (RCT) (Yang & Parvin, 2003), which transports boundary points to the local center of mass iteratively. This can be classified as curve-based voting, since the voting path is not along a straight line but along a minimum energy path. Voting paths can be easily distorted by noise, local structures, and other singularities in the image, and may lead to over-segmentation. Thus, the problem is often regularized at different levels through either non-linear diffusion of random noise (Perona & Malik, 1990), non-linear diffusion of speckle noise (Yang & Parvin, 2003), or enforcing smoothness of the path leading each point on the surface to its local centroid (Yang & Parvin, 2003).

The first two categories of radial symmetry detection can be summarized as follows. Interest-point operators are fast and well-suited for detecting small features for higher levels of interpretation and manipulation. Parametric voting techniques are potentially memory-intensive, depending upon the dimensionality of the parameter space, and remain sensitive to small deviations from the underlying geometric model. Line- and area-based voting produce a voting space that is diffuse and subject to further ad hoc analysis.

The method implemented here falls into the category of iterative techniques that are adaptive to geometric perturbation and typically produce more stable results. This method shares several attributes with tensor-based voting (Medioni et al., 2000), but it differs in that it is scalar and iterative.

4 Segmentation

In a typical 2D cell culture assay that is stained for nuclear compartment, some nuclei are isolated and others are clustered together to form clumps. Thus, the strategy is to detect isolated ones first, and then impose additional processing for the clumped regions. The image signature suggests that thresholding may be sufficient as an initial step; however, shading, nonuniform staining, and other artifacts demands a localized strategy. This localized strategy is an edge-based technique with a geometric convexity optimization approach for improved reliability. Edges are collected to form contours and then tested for convexity. If convexity fails then the clumped region is partitioned into multiple convex regions according to a geometric policy. Contour division is initiated from points of positive maximum curvature that are detected from contours. At the resolution that samples are imaged, showing the morphology of epithelial cells (round cells) used in the experimental design, there is often a clear positive curvature maxima where adjacent nuclei overlap. Curvature is often computed by convolving the contour with the first and second derivative of a Gaussian kernel. The kernel scale (standard deviation) has to be matched with

the resolution and numerical aperture of the objective for optimum performance.

4.1 Boundary extraction and convexity

Let $I(x, y)$ be the original image with 2D image coordinates. An initial boundary is extracted by linking zero-crossing edges that are filtered by the gradient magnitude at the same scale. Zero-crossing (computed from Laplacian, $\nabla^2 I$) assures that boundaries are closed, and the gradient threshold assures that spurious contours are eliminated. Two gradient thresholds (low and high) are used to initiate linking from strong edges and fill the gaps with weak edge points. Next, each computed contour is approximated with a polygon and total angular change is computed to test for convexity. If the region is not convex then additional processing is initiated.

4.1.1 Grouping and Partitioning

Partitioning of clumped nuclei into distinct convex objects is through iterative decomposition and constraint satisfaction. Intuitively, these partitions should be terminated by folds in the boundary corresponding to positive curvature maxima. The main purpose of the constraint-based grouping is to limit the number of hypotheses and reduce computational cost. The net result of this process is a set of corresponding candidates for each positive curvature maxima point for potential decomposition. The following geometric constraints are enforced.

Positive curvature constraint The curvature (Faux & Pratt, 1979) at any point along the contour is given by $k = \frac{\delta' x \delta'' y - \delta' y \delta'' x}{(\delta' x^2 + \delta' y^2)^{3/2}}$. The contour derivatives are computed by convolving derivatives of a Gaussian with the contour information. The intent is to partition a clump of nuclei from the points of maximum curvature along the contour.

Antiparallel constraint The antiparallel constraint asserts that each pair of positive curvature maxima along the contour must be antiparallel, which is estimated by computing the tangent directions at each candidate point. This constraint reduces the number of hypotheses for a potential partition thus reducing the computational cost.

Non-intersecting constraint The non-intersecting constraint asserts that a partition cannot intersect existing boundaries corresponding to the entire blob or other hypothesized partitions.

Convexity constraint The nuclear regions that occur in the cell culture are always convex, the convexity constraint enforces that the partition obtained has to be convex to avoid incorrect segmentation.

Grouping and partitioning Each clump is partitioned by linking pairs of positive curvature maxima that satisfy the above conditions. Each configuration has its own cost function, and the optimum configuration satisfies all the above-mentioned constraints and will minimize

$$C = \Sigma_{i=1}^{n} \frac{\phi_i - \Pi}{\Pi} \tag{1}$$

where n is the number of partitions in a clump and ϕ_i is the convexity of the compartment, is determined by the system as follows. Essentially, the problem is reduced to grouping of curvature maximas in such a way that certain geometric constraints are satisfied.

Decomposition Algorithm

1. Localize positive curvature maxima along the contour

2. Set initial number of compartments n:= 2

3. Construct a set of all valid configurations of n compartments by connecting valid pairs of positive curvature maxima satisfying the antiparallel, non-intersecting and convexity constraints

4. Evaluate cost of each configuration (per Equation 1)

5. Increment the compartment count n:=n+1 and repeat steps 3 and 4 until there is at least one configuration that has all convex compartments

6. Select the configuration with the least cost function

The algorithm outlined above can be used to partition varying numbers of touching blobs. Figure 1 shows three touching blobs and outlines the mechanism by which the various constraints elucidate partition of touching nuclei. The decomposition of four touching nuclei in real data is shown in Figure 6e.

4.2 Experiment with noisy data

The sensitivity of the segmentation algorithm was tested by adding Gaussian additive noise to a synthetic image. The amount of Gaussian noise was varied and the segmented area was measured against a known ground truth area of 20697 pixels. The results of the segmentation is shown in Figure 3. It can be seen that segmentation obtained is not affected by the presence of noise when Gaussian additive noise is varied from 5% to 40%. Incorrect segmentation is obtained when Gaussian additive noise is varied above 50%. The area obtained from segmentation is shown in Table 1.

5 Protein localization

The problem of localizing punctate protein expression was first evaluated using the Hough transform, cross correlation against training samples, and analysis of local intensity distribution. Clustering based

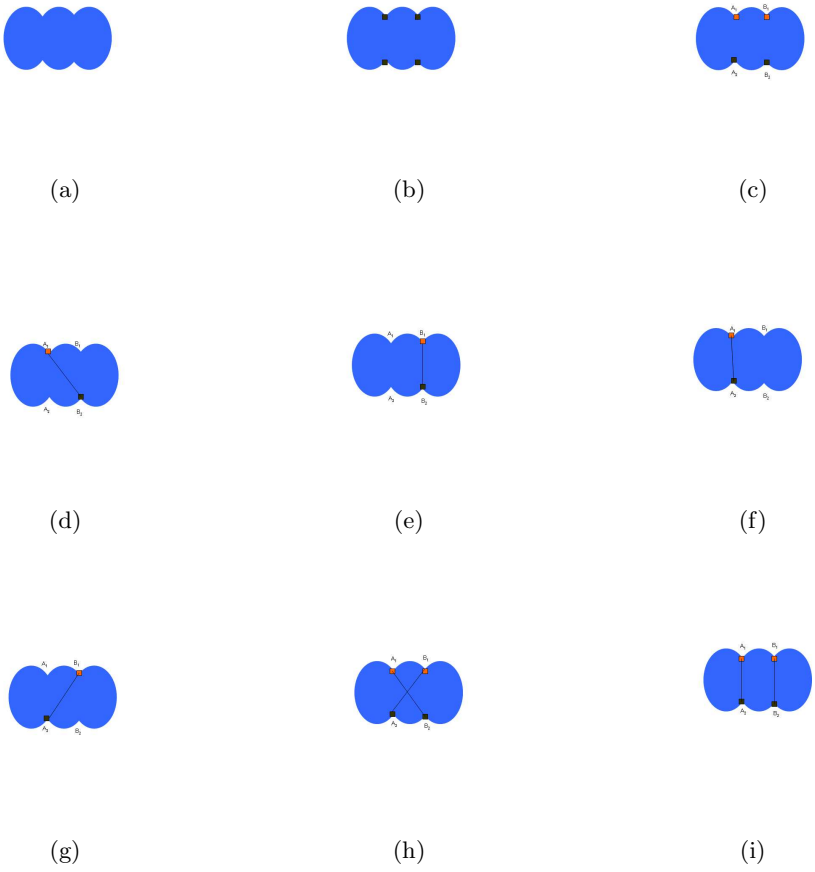

(a) (b) (c)

(d) (e) (f)

(g) (h) (i)

Figure 1: Graphical representation showing optimal partitioning by applying the constraints: (a) Visualization of three touching blobs; (b) localize the positive curvature maxima; (c) anti-parallel constraint to reduce number of hypotheses; (d)-(g) computed partition fails due to convexity constraint; (h) computed partition fails due to non-intersecting constraint and (i) computed partition which satisfies all the constraints.

Image	*Area in Pixels*
Figure 3a	26228
Figure 3b	26228
Figure 3c	26228
Figure 3d	26228
Figure 3e	25905
Figure 3f	26228
Figure 3g	25896
Figure 3h	25912

Table 1: Image and corresponding computed area as a function of increasing noise

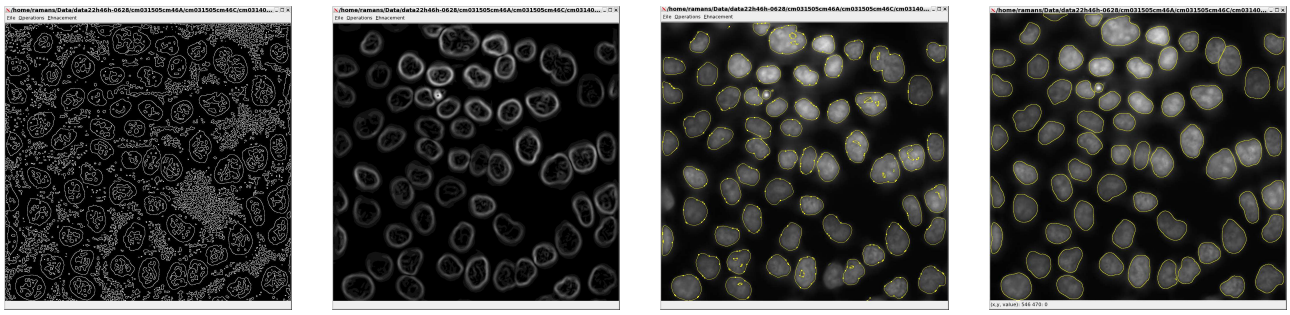

(a) (b) (c) (d)

Figure 2: Steps in segmentation: (a) Zero-crossing of Laplacian; (b) gradient image; (c) points of maximum curvature along contours; and (d) partitioning of clumped nuclei.

on the Hough method proved to be scale-sensitive, while correlation and intensity-based methods suffer from false positives and lack of geometric models. A geometric model is essential in the presence of scale-varying and overlapping protein signals. A new type of spatial iterative voting is introduced to facilitate these requirements (Yang & Parvin, 2004). Voting along gradient direction provides a hypothesis profile for saliency, e.g., punctate protein events. A specific kernel design (1) encodes the knowledge for saliency, (2) is applied at each edge location along the gradient direction, and (3) is refined and reoriented at each iteration step. The shape and evolution of these kernels, inferring center of mass, is shown in Figure 4. A brief review of the technique is as follows: Let $I(x, y)$ be the original image, where the domain points (x, y) are 2D image coordinates. Let $\alpha(x, y)$ be the voting direction at each image point, where $\alpha(x, y) := (\cos(\theta(x, y)), \sin(\theta(x, y)))$ for some angle $\theta(x, y)$ that varies with the image location. Let $\{r_{\min}, r_{\max}\}$ be the radial range and Δ be the angular range. Let $V(x, y; r_{\min}, r_{\max}, \Delta)$ be the vote image, dependent on the radial and angular ranges and having the same dimensions as the original image. Let $A(x, y; r_{\min}, r_{\max}, \Delta)$ be the local voting area, defined at each image point (x, y) and dependent on the

radial and angular ranges, defined by

$$\begin{aligned} A(x,y;r_{\min},r_{\max},\Delta) \;:=\; & \{(x \pm r\cos\phi, y \pm r\sin\phi) \mid r_{\min} \le r \le r_{\max} \text{ and} \\ & \theta(x,y) - \Delta \le \phi \le \theta(x,y) + \Delta\} \end{aligned} \tag{2}$$

Finally, let $K(x,y;\sigma,\alpha,A)$ be a 2D Gaussian kernel with variance σ, masked by the local voting area $A(x,y;r_{\min},r_{\max},\Delta)$ and oriented in the voting direction $\alpha(x,y)$. Figure 4 shows a subset of voting kernels that vary in topography, scale, and orientation.

The iterative voting algorithm is outlined below for radial symmetry.

Iterative Voting

1. *Initialize the parameters:* Initialize $r_{\min}, r_{\max}, \Delta_{\max}$, and a sequence $\Delta_{\max} = \Delta_N < \Delta_{N-1} < \cdots < \Delta_0 = 0$. Set $n := N$, where N is the number of iterations, and let $\Delta_n = \Delta_{\max}$. Also fix a low gradient threshold, Γ_g and a kernel variance, σ, depending on the expected scale of salient features.

2. *Initialize the saliency feature image:* Define the feature image $F(x,y)$ to be the local external force at each pixel of the original image. The external force is often set to the gradient magnitude or maximum curvature, depending upon the type of saliency grouping and the presence of local feature boundaries.

3. *Initialize the voting direction and magnitude:* Compute the image gradient, $\nabla I(x,y)$, and its magnitude, $||\nabla I(x,y)||$. Define a pixel subset $S := \{(x,y)|\ ||\nabla I(x,y)|| > \Gamma_g\}$. For each grid point $(x,y) \in S$, define the voting direction to be

$$\alpha(x,y) := -\frac{\nabla I(x,y)}{||\nabla I(x,y)||}$$

4. *Compute the votes:* Reset the vote image $V(x, y; r_{\min}, r_{\max}, \Delta_n) = 0$ for all points (x, y). For each pixel $(x, y) \in S$, update the vote image as follows:

$$\begin{aligned} V(x, y; r_{\min}, r_{\max}, \Delta_n) \quad := \quad & V(x, y; r_{\min}, r_{\max}, \Delta_n) + \\ & \textstyle\sum_{(u,v)\in A(x,y;r_{\min},r_{\max},\Delta_n)} F(x - \frac{w}{2} + u, y - \frac{h}{2} + v) K(u, v; \sigma, \alpha, A), \end{aligned}$$

where $w = \max(u)$ and $h = \max(v)$ are the maximum dimensions of the voting area.

5. *Update the voting direction:* For each grid point $(x, y) \in S$, revise the voting direction. Let

$$(u^*, v^*) = \arg \max_{(u,v)\in A(x,y;r_{\min},r_{\max},\Delta_n)} V(u, v; r_{\min}, r_{\max}, \Delta_n)$$

Let $d_x = u^* - x, d_y = v^* - y$, and

$$\alpha(x, y) = \frac{(d_x, d_y)}{\sqrt{d_x^2 + d_y^2}}$$

6. *Refine the angular range:* Let $n := n - 1$, and repeat steps 4-6 until $n = 0$.

7. *Determine the points of saliency:* Define the centers of mass or completed boundaries by thresholding the vote image:

$$C = \{(x, y) \mid V(x, y; r_{\min}, r_{\max}, \Delta_0) > \Gamma_v\}$$

An example of the application of radial kernels to overlapping objects is shown in Figure 5 together with the intermediate results. The voting landscape corresponds to the spatial clustering that is initially diffuse and subsequently refined and focused into distinct islands.

6 Experimental results and conclusion

The algorithms presented in sections 4 and 5 have been packaged into a stand alone software tool for routine quantitative studies. The tool has been used to study centrosomal abnormalities under different treatment groups. Figure 6 shows the performance of the system on overlapping nuclear regions. It should be noted that in some cases there is no intensity decay when adjacent nuclei overlap; watershed-based techniques can fail to produce proper decomposition of nuclear compartments under these conditions. In contrast, the proposed geometric approach is invariant to intensity distribution as a basis for decomposition. An example of localization of centrosomes through voting is shown in Figure 7, where a rare event due to CA is captured in region 20 and region 45. Each punctate signal is assigned to the closest nuclear boundary. A total of 196 images were processed to quantify the number of abnormal centrosomes for each nucleus in the image. This result was then compared against manual count for validation, as shown in Figure 8. The system's error is at 1% and 10% for nuclear segmentation and quantitation of centrosome abnormality, respectively. This is a significant improvement in productivity for high throughput analysis.

References

Chan, G.K., Jablonski, S.A., Sudakin, V., Hittle, J.C. & Yen, T.J. (1999) Human bubr1 is a mitotic checkpoint kinase that monitors cenp-e functions at kinetochores and binds the cyclosome/apc. *J. Cell Biol.* 146, 941–954.

Duda, R.O. & Hart, P.E. (1972) Use of the hough transform to detect lines and curves in pictures. *Comm. Assoc. Comp. Mach.* 15, 11–15.

I.D. Faux & M.J. Pratt. (1979) *Computational geometry for design and manufacture.* Ellis Horwood, Chichester, England.

Loy, G. & Zelinsky, A. (2003) Fast radial symmetry for detecting points of interest. *IEEE Trans. Pattern Anal. Mach. Intell.* 25, 959–973.

Malladi, R. & Sethian, J. (1996) A unified approach to noise removal, image enhancement, and shape recovery. *IEEE*

Trans. Image Processing 5, 1554–1568.

Medioni, G., Lee, M.S. & Tang, C.K. (2000) A Computational Framework for Segmentation and Grouping. *Elsevier*, New York, USA.

Minor, L.G. & Sklansky, J. (1981) The detection and segmentation of blobs in infrared images. *IEEE Trans. Syst. Man Cybern.* 11, 194–201.

Murphy, R. (2004) Automated interpretation of subcellular location patterns. In *IEEE Int. Symp. Biomedical Imaging* ISBI 2004, 53–56.

Ortiz De Solorzano, C., Malladi, R., Lelievre, S.A. & Lockett, S.J. (2001) Segmentation of nuclei and cells using membrane related protein markers. *J. Microsc.* 201, 404–415.

Parvin, B., Yang, Q., Fontenay, G. & Barcellos-Hoff, M.H. (2003) Biosig: An imaging bioinformatics system for phenotypic analysis. *IEEE Trans. Syst. Man Cybern.* 33, 814–824.

Perona, P. & Malik, J. (1990) Scale space and edge detection using anisotropic diffusion. *IEEE Trans. Pattern Anal. Mach. Intell.* 12, 629–640.

Reisfeld, D., Wolfson, H. & Yeshurun, Y. (1995) Context-free attentional operators: The generalized symmetry transform. *Int. J. Comp. Vision* 14, 119–130.

Reisfeld, D. & Yeshurun, Y. (1998) Preprocessing of face images: Detection of features and pose normalization. *Comp. Vision Image Understanding* 71, 413–430.

Salisbury, J.L. (2001) The contribution of epigenetic changes to abnormal centrosomes and genomic instability in breast cancer. *J. Mamm. Gland Biol. Neoplasia* 6, 203–12.

Salisbury, J.L., D'Assoro, A.B. & Lingle, W.L. (2004) Centrosome amplification and the origin of chromosomal instability in breast cancer. *J. Mamm. Gland Biol. Neoplasia* 9, 275–83.

Sela, G. & Levine ,M.D. (1997) Real-time attention for robotic vision. *Real-Time Imaging* 3, 173–194.

Vincent, L. & Soille, P. (1991) Watersheds in digital spaces: An efficient algorithm based on immersion simulations. *IEEE Trans. Pattern Anal. Mach. Intell.* 13, 583–598.

Yang, Q. & Parvin, B. (2003) Harmonic cut and regularized centroid transform for localization of subceullar structures. *IEEE Trans. Biomed. Engineering* 50, 469–475.

Yang, Q. & Parvin, B. (2004) Perceptual organization of radial symmetries. In *Proc. Conf. Computer Vision and Pattern Recognition* 1, 320–325.

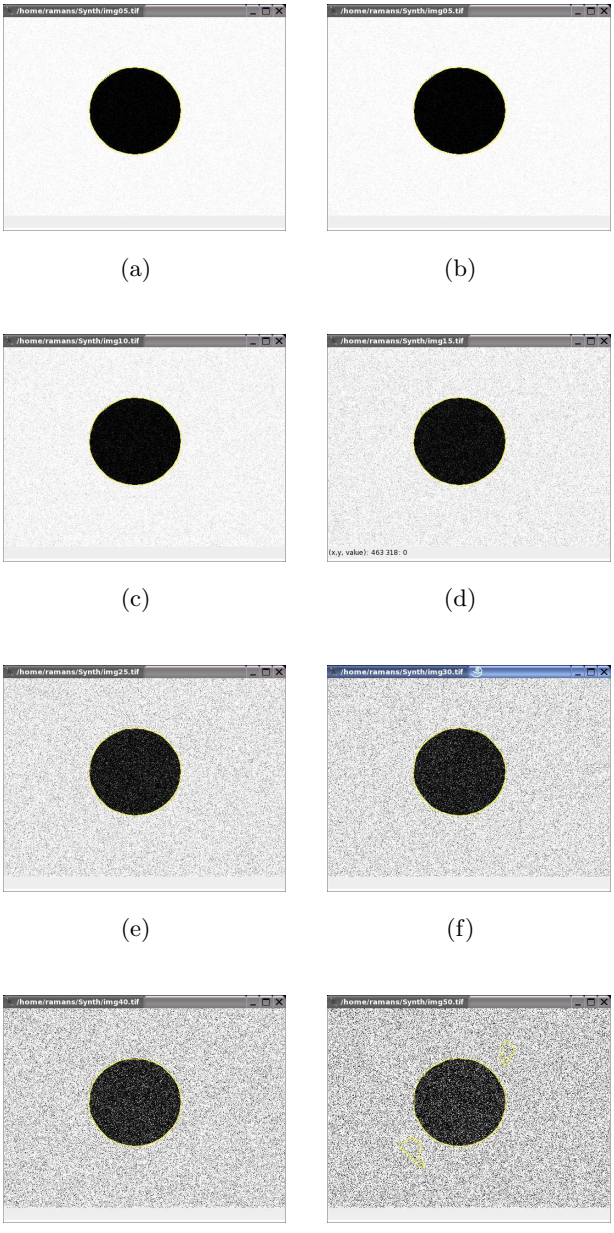

Figure 3: Segmentation of a synthetic object with added Gaussian noise: (a) no noise; (b) 5% additive noise; (c) 10% additive noise; (d) 15% Gaussian additive noise; (e) 25% Gaussian additive noise; (f) 30% Gaussian additive noise; (g) 40% Gaussian additive noise; (h) 50% Gaussian additive noise generates additional fragments.

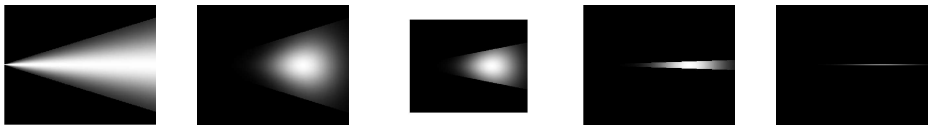

(a) (b) (c) (d) (e)

Figure 4: Kernel topography: (a-e)The evolving kernel, used for the detection of radial symmetries (shown at a fixed orientation), has a trapezoidal active area with Gaussian distribution along both axes.

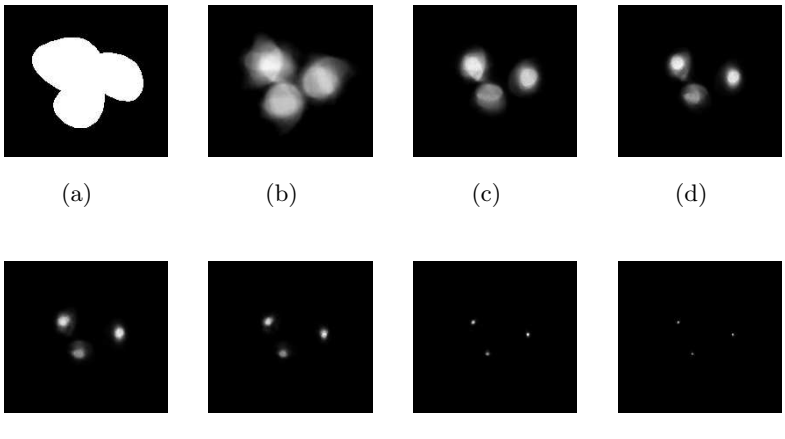

(a) (b) (c) (d)

(e) (f) (g) (h)

Figure 5: Detection of radial symmetries for a synthetic image simulating three overlapping centrosomes (a protein event): (a) original image; (b)-(g) voting landscape at each iteration; and (h) final localization of centers of mass.

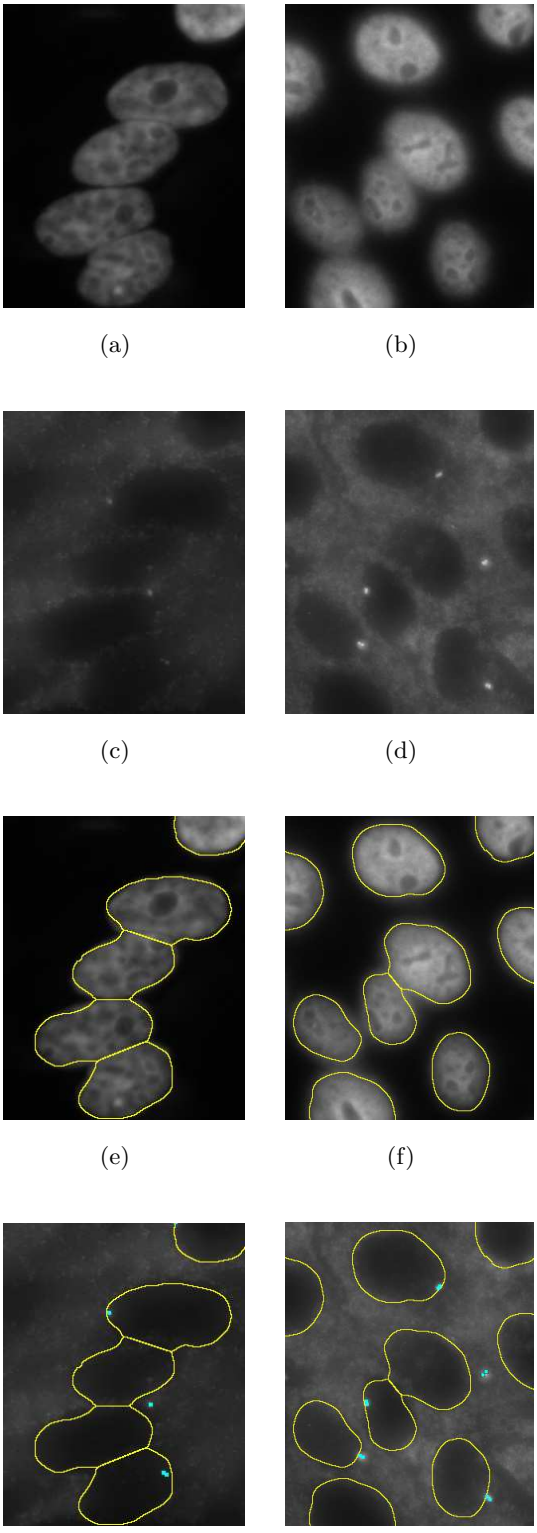

Figure 6: Decomposition of overlapping nuclei and detection of punctate events corresponding to centrosome complexes: (a) and (b) original DAPI stained nuclear images; (c) and (d) corresponding centrosome signature; (e) and (f) segmentation and decomposition of nuclear compartments; (g) and (h) localized centrosomes. Nuclear and centrosome regions are labeled with yellow and cyan colors respectively.

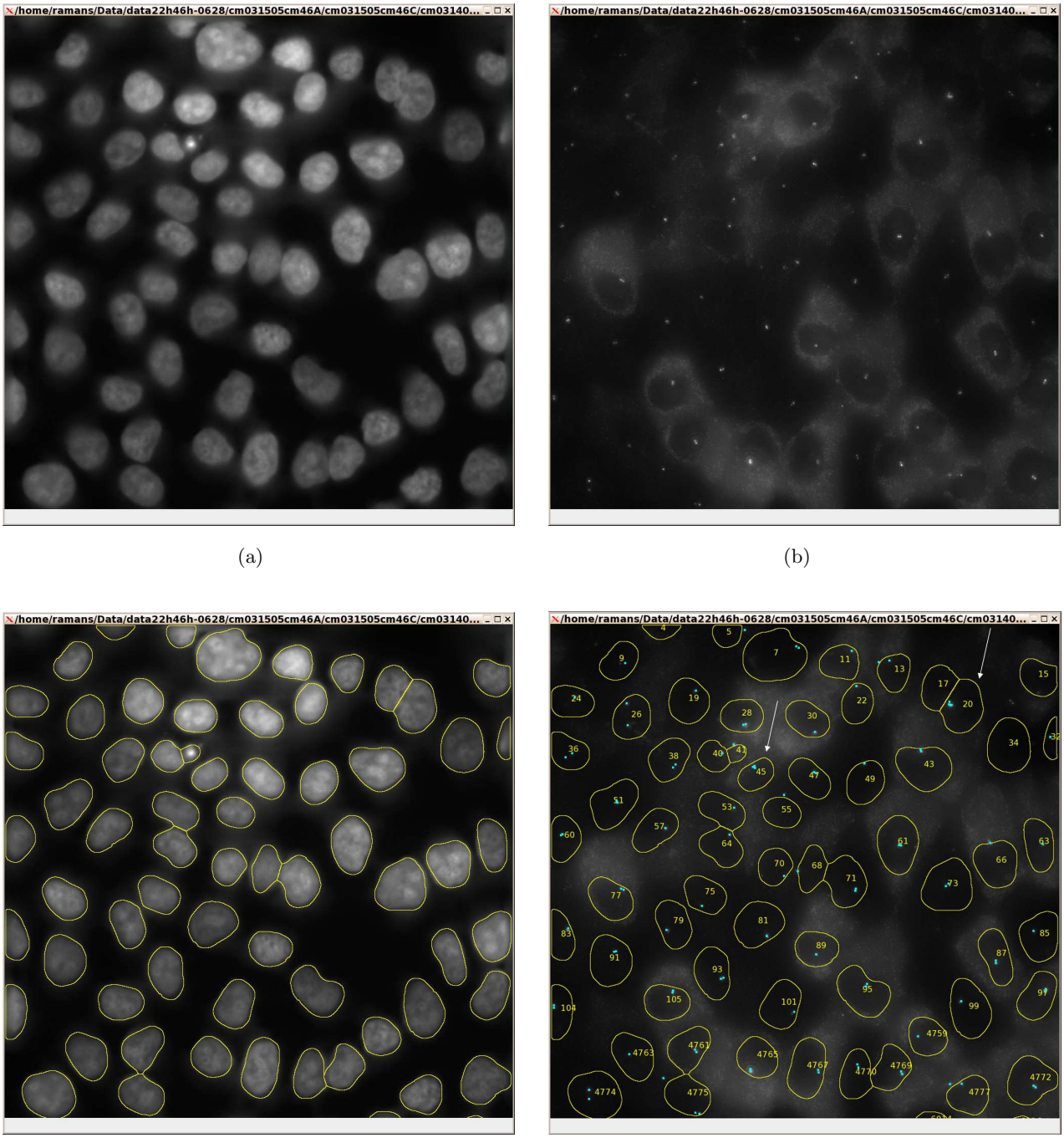

Figure 7: Nuclear segmentation and centrosome localization indicates decomposition of overlapping nuclear compartments and detection of nearby punctate events corresponding to centrosome: (a) original nuclear image; (b) corresponding centrosomes image; (c) segmented nuclear compartments; and (d) localized centrosomes. A rare event in nuclei 20 and 45 indicates four and three centrosomes, respectively. Nuclear and centrosome regions are labeled with yellow and cyan colors, respectively. Ambiguities due to adjacent and overlapping regions (both nuclear and centrosomes) are resolved. Furthermore, pertinent events are measured in context. For example, centrosome abnormality of region 20 is referenced against correct nuclear size of morphology.

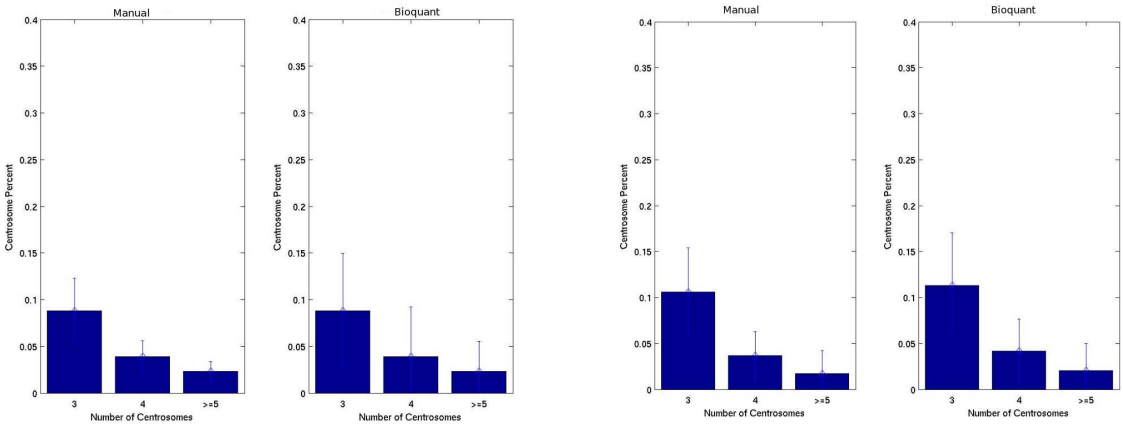

(a) (b)

Figure 8: Comparative results of centrosome abnormality between manual and automated counting for two separate treatments. Each chart shows manual (on the left) and automated quantitation (on the right).